ELSEVIER

Cement & Concrete Composites 26 (2004) 563–572

Cement & Concrete Composites

www.elsevier.com/locate/cemconcomp

# Early-age stress–crack opening relationships for high performance concrete

Lennart Østergaard [a,*], David Lange [b], Henrik Stang [a]

[a] Department of Civil Engineering, Technical University of Denmark, DK-2800, Kgs. Lyngby, Denmark
[b] University of Illinois at Urbana-Champaign, 2122 NCEL, MC-250, Urbana, IL 61801, USA

**Abstract**

Stress–crack opening relationships for concrete in early age have been determined for two high performance concrete mixes with water to cementitious materials ratios of 0.307 and 0.48. The wedge splitting test setup was used experimentally and the cracked non-linear hinge model based on the fictitious crack model was applied for the interpretation of the results. A newly developed inverse analysis algorithm was utilized for the extraction of the stress–crack opening relationships. Experiments were conducted at 8, 10, 13, 17, 22, 28, 48, 168 h (7 days) and 672 h (28 days). At the same ages, split tests were carried out. Fracture energy, $G_f$, was found to increase with age, while the characteristic length, $l_{ch}$, was found to decrease.


*Keywords:* Stress–crack opening relationship; Fictitious crack model; Inverse analysis; Early age; High performance concrete

## 1. Introduction

The use of the fictitious crack model originated by Hillerborg et al. [1] for the modelling of crack initiation and propagation in concrete has been widespread and accepted in the research community for the last two decades. This is due to the fact that this model is able to closely describe the fracture behavior of concrete, and because it gives a good understanding for many previously unexplained phenomenas, like e.g. the size effect. However, one problem in the use of the model is that it requires knowledge of the stress–crack opening relationship, $\sigma_w(w)$. Determination of this property has been a problem until recently. Usually in literature, only the fracture energy, $G_f$, has been determined and from this value a prescribed function for $\sigma_w(w)$ has been calibrated. However, also the shape of $\sigma_w(w)$ is important for the determination of the risk of cracking in early age.

Determination of the early-age development of the fracture mechanical parameters for concrete has been investigated by some authors in the literature. Petersson [2], conducted experiments on normal concrete, varying among other factors water–cement ratio and age at testing. Three point bending tests were performed at 2, 7, 28 and 91 days on a mix with a water–cement ratio of 0.50. It was found that the fracture energy increases with age, while the characteristic length decreases in the period of 2–28 days. Brameshuber and Hilsdorf [3,4], conducted three point bending experiments from 4 h until 28 days with a water–cement ratio of 0.54. An increase of fracture energy with age was found, while the characteristic length was found to be small in the very early age (4 h), then reaching a maximum 1 h later, followed by a minimum and a new maximum, whereafter it decreased with age. Wittmann et al., [5], investigated the influence of water–cement ratio and age at loading for concrete using the three point bending test. The age was varied from 2 to 28 days while the selected water–cement ratios were 0.40–0.65. This paper represents the only work in literature, where the shape of the softening curve with age is determined. A program was used to extract the softening curve (assumed bilinear) from the experimentally obtained load–deflection curves. An increase in $G_f$ was found while $l_{ch}$ decreased with age. Zollinger et al., [6] investigated fracture toughness with a water–cement ratio of 0.53 from 12 h until 28 days. It was found that the fracture toughness increases with age, while the length of the fracture process zone, $c_f$, decreases. It is concluded that concrete at very early age (12 h) is more brittle than concrete at

* Corresponding author. Tel.: +45-45-25-1861; fax: +45-45-88-3282.
*E-mail address:* los@byg.dtu.dk (L. Østergaard).

0958-9465/$ - see front matter © 2003 Elsevier Ltd. All rights reserved.
doi:10.1016/S0958-9465(03)00074-X

28 days. Schutter and Taerwe [7], investigated the development of fracture energy at early ages as a function of the degree of hydration. The age at testing ranged from 1 to 28 days. It was found that $G_f$ increases with age, while $l_{ch}$ is reported to develop in the same way as found in [3]. Gettu et al., [8] investigated high strength concrete with a water–cementitious materials ratio of 0.25 at ages from 4 to 232 days. It was concluded that the fracture energy and toughness decreases with age, while the brittleness increases. Hariri, [9], has investigated the development of fracture mechanical properties and the width of the fracture process zone of early-age concrete. It was found that $G_f$ increases, while $l_{ch}$ decreases with age.

Some general conclusions may be drawn from the literature. In general it has been found that the fracture energy increases with age while the characteristic length decreases. The only detailed study of the development of fracture energy and characteristic length in very early age was performed by Brameshuber and Hilsdorf [3,4], whose conclusions follow the majority of the work in the literature. Only one paper has determined the shape of the stress–crack opening relationship in early age [5]. They assumed a bilinear $\sigma_w(w)$-curve and found that both the first and the second slope of this relation decreases with age (cf. sign-definition in Fig. 4). Also the intersection with the ordinate was found to decrease.

In this paper results from experiments concerning the development of tensile strength, stiffness and shape of the stress–crack opening relationship with age of very young concrete are presented. The wedge splitting test first described by Tschegg [10], see also Rossi et al., [11] is used, while the results are interpreted using the non-linear cracked hinge model first introduced by Ulfkjær et al., [12] and further developed by Olesen and Stang [13–15]. The model was adapted to the wedge splitting test by Østergaard et al., [16] who also developed an algorithm for inverse analysis, thereby making an objective determination of the stress–crack opening relationship possible. The theory is briefly described in the following.

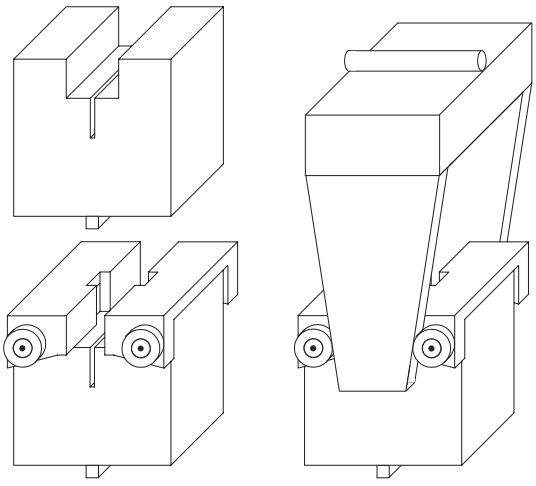

Fig. 1. Upper left: specimen placed on line support; lower left: mounting of two loading devices with roller bearings; right: wedge in place between roller bearings.

## 2. Modelling

Fig. 1 shows the principal experimental setup. Loading of the wedge results in a splitting force acting on the specimen, which at a certain load level result in the initiation and subsequent stable propagation of a crack at the bottom of the notch. The experiment may be controlled both in closed loop crack mouth opening displacement (CMOD) control or by constant rate of displacement of the wedge, where the latter is acceptable due to the stability of the crack propagation. The vertical loading of the wedge and the CMOD, using a clip gage, are recorded during experiments and used in the

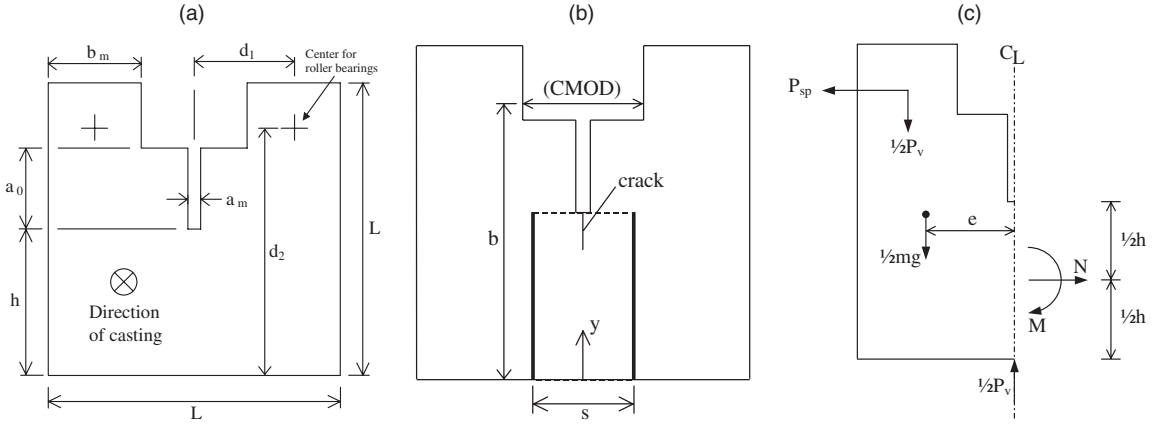


Fig. 2. Geometry and loading of the WST-specimen (a), incorporation of the hinge element (b) and loading (c).

analysis. Fig. 2a shows the geometry of the WST-specimen in more detail. The side length of the cube is $L$ and the thickness, $t = L$. The initial notch length is $a_0$ while the ligament length is $h$. The coordinates for the center of the roller bearings are described by $d_1$, which is the horizontal distance from the centerline, and $d_2$, the distance from bottom of the specimen. These must be known since the resultant of the wedge forces go through this point.

The concept of the hinge is to view the crack as a local discontinuity in the overall stress and strain field. This change is assumed to vanish outside a certain bandwidth, $s$. Within this band, modelling of the crack takes place, and outside, the structural element is modelled using the appropriate elastic theory. Incorporation of the hinge element in the wedge splitting specimen opens up for fast interpretation of this experimental setup. Fig. 2b shows how the hinge element is incorporated into the WST-specimen. As shown, the hinge is placed upside down with crack initiation at the bottom of the notch. The crack mouth opening displacement, CMOD, is calculated at a distance $b$ from the bottom of the specimen.

The hinge itself is modelled by viewing it as incremental layers of independent springs, attached to the boundaries of the element. The boundaries of the hinge are assumed to be rigid and may rotate and translate, see Fig. 3. In this way, the hinge may be used in e.g. three point bending beams and for wedge splitting specimens. The constitutive relationship for each spring is assumed to be linear elastic in the pre-crack state, while the cracked state is approximated by a bilinear $\sigma_w(w)$-curve, see Fig. 4.

Analysis of the hinge element makes it possible to determine the internal normal force, $N$, and bending moment, $M$, for any given value of the angular hinge deformation, $2\varphi$. These formulas are given in Olesen [13]. The problem is solved in four phases, one for each state of crack propagation. Phase 0 represents the elastic state, where no crack has formed, while phases I, II and III represent different stages of propagation (linear, bilinear and bilinear with stress-free tail). The solution is

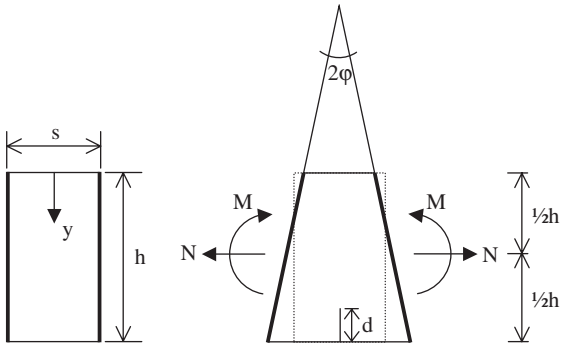


Fig. 3. Geometry, loading and deformation of the hinge element.

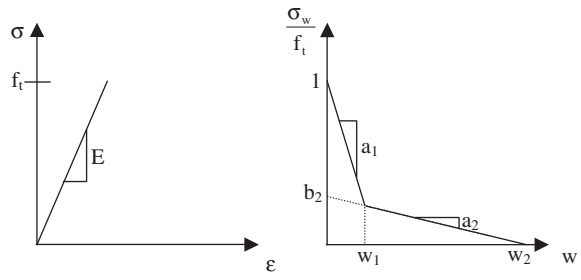


Fig. 4. Stress–strain relationship in pre-crack state (a) and stress–crack opening relationship in cracked state (b). $E$ = elastic modulus; $\varepsilon$ = elastic strain; $\sigma_w(w)$ denotes the stress–crack opening relationship with $w$ = crack opening; and $f_t$ = tensile strength.

presented in terms of normalized properties, where the following normalizations are used:

$$\mu = \frac{6}{f_t h^2 t} M, \quad \rho = \frac{1}{f_t h t} N, \quad \theta = \frac{hE}{s f_t}\varphi, \quad \alpha = \frac{d}{h} \tag{1}$$

where $t$ is the hinge thickness. Given these normalizations, the pre-crack behavior of the hinge is described by $\alpha = 0$ and $\mu = \theta$. Fig. 2c shows the loading of the WST-specimen. The resultant acting on the specimen from the roller bearings is resolved into a splitting part and a vertical part. The figure also shows loading due to self-weight, $mg$, acting a distance, $e$, from the centerline. Usually, self-weight of WST-specimens is ignored in the interpretation of experimental results, since for mature samples the influence is vanishing. However, if experiments are performed on samples in early-age self-weight should be considered. Finally, Fig. 2c also shows the sectional forces acting in the symmetry plane. From Fig. 2c, expressions for the external moment, $M$, and the normal force, $N$, in the symmetry plane may be determined from the equilibrium equations:

$$N = P_{sp} \tag{2}$$

$$M = P_{sp}\left(d_2 - \frac{h}{2}\right) + \frac{1}{2}P_v d_1 + \frac{1}{2}mge \tag{3}$$

where $m$ = mass of specimen and $g$ = gravity. Analysis in all phases of crack propagation is performed by balancing the internal moment and normal force in the hinge for a given prescribed hinge rotation by the external forces given by (2) and (3). Then, CMOD is calculated based on the results of this analysis. The latter depends on three different contributions. These are the opening due to elastic deformation, $\delta_e$, opening due to the presence of the crack, $\delta_{COD}$, and opening due to the distance between the load line and the crack mouth at the bottom of the notch, $\delta_g$. Thus, CMOD, is given by

$$\text{CMOD} = \delta_e + \delta_{COD} + \delta_g \tag{4}$$

The first term in Eq. (4) may be determined from handbooks on stress analysis of cracks. According to Tada et al. [17], $\delta_e$ is given by

$$\delta_e = \frac{P_{sp}}{Et}\frac{x}{(1-x)^2}(38.2 - 55.4x + 33.0x^2) \quad (5)$$

where $x = 1 - h/b$. The opening due to the presence of the crack is derived by Olesen [13], and is given by

$$\delta_{COD} = \frac{sf_t}{E}\frac{1 - b_i + 2\alpha\theta}{1 - \beta_i} \quad (6)$$

where $b_i$, and $\beta_i = (f_t a_i s)/E$ must be chosen in accordance with the actual phase of crack propagation. The opening due to the distance between the load line and the bottom of the notch, may be calculated using the mean angle of the crack phases and the distance from the top of the crack to the gage [16]:

$$\delta_g = 2\overline{\varphi}_{cr}(b-h) = 2(b-h)\left(\frac{\delta_{COD}}{2\alpha h} - \frac{sf_t}{hE}\frac{\theta_{0-I}}{1-\beta_1}\right) \quad (7)$$

where $\overline{\varphi}_{cr}$ is the mean crack angle. The constant term in Eq. (7) is caused by the hinge model and is an artifact of the model, see e.g. [16]. Derivation of Eqs. (6) and (7) is described shortly in Appendix A. Note, that for large values of $\beta_1$ another solution for the hinge element must be applied (drop-linear), see [13].

The inverse analysis uses a phased approach, where only the parameters governing the response of a particular phase are free, while the other parameters are fixed. The method is developed by Østergaard et al., [16]. For example, in the linear elastic phase, only the modulus of elasticity has an influence on the load–CMOD curve, and thus, only this parameter is free. In phase I, only tensile strength, $f_t$, initial slope of the stress–crack opening relationship, $a_1$, and modulus of elasticity, $E$, has influence on the response. But since $E$ is known, the optimization may be performed for $f_t$ and $a_1$ only. Finally, for phases II and III, all parameters are fixed except for $a_2$ and $b_2$. This method is dependent on good initial guesses for the fixed parameters when the optimization for a particular parameter is performed. If such guesses are unknown, the method will still converge if a few runs are performed. The optimization was performed using the sum of squares as object function:

$$\min_p \quad \frac{1}{N}\sum_0^N (P_{sp} - \widehat{P}_{sp})^2 \quad \text{s.t.} \quad p_{min} < p < p_{max} \quad (8)$$

where $N$ is the total number of observations in the entire data set, and $p$ is a vector of parameters, which is optimized for in a particular phase. Optimization for $E$ was found to be very stable and a local minimum was never encountered. It was also found that no local minima exists when optimizing for $f_t$ and $a_1$, [16], nor when optimizing for $a_2$ and $b_2$. The object functions proposed by Ulfkjær et al., [12] were tested but it was concluded that Eq. (8) performs satisfying. The algorithm was written in MatLab using the simplex method. Equidistant experimental observations were selected from the full data set, and predictions were calculated from the model at the same CMOD values. If, for any reason, the distance between two experimental observations was greater than 1.5 times the desired distance, a linear interpolation scheme was used to fill the gap. The validity of the proposed way of calculating the load–CMOD curve and the method for inverse analysis has been explored in a finite element model, [16], and it produces good results. Note, that the choice of bandwidth parameter, $s$, influences the results from the inverse analysis, see [16]. Thus, an initial calibration of the bandwidth parameter using a finite element model is beneficial for the precision. This has been done in the present paper. However, the influence is weak, and the calibration may be skipped. For details, see [16].

## 3. Experimental procedure

The mix designs were chosen similar to the mixes used in the Danish HETEK research program on the determination of the early-age properties of high performance concrete [18,19]. The mix designs are shown in Table 1. The two mixes are identical except for the change in water to cementitious materials ratio and the fact that addition of superplasticizer was necessary in mix I. This fact resulted in a retardation of mix I in the very early age (8–10 h) that was not present in mix II.

The concrete was mixed using a continuous pan mixer. First, the dry materials were mixed for 2 min, then water was added and the mixing continued for another minute before the admixtures were added. Total mixing time was 5 min.

Cylinders for determination of the split tensile strength were cast in PVC molds, while WST-specimens

Table 1
Mix designs (kg/m$^3$)

| Mix | I | II |
|---|---|---|
| Cement (ASTM Type III) | 310.0 | 242.0 |
| Fly ash (F) (20% of cement weight) | 62.0 | 48.4 |
| Silica fume (5% of cement weight) | 15.5 | 12.1 |
| Water | 112.8 | 144.2 |
| Air entraining agent (0.1% of cement weight) | 0.388 | 0.303 |
| Plasticizer (0.6% of cement weight) | 2.33 | 1.82 |
| Superplasticizer (1.6% of cement weight) | 6.2 | 0.0 |
| FA, sea gravel, 00–04 mm | 783.0 | 781.0 |
| CA, sea gravel, 04–08 mm | 343.7 | 342.9 |
| CA, sea gravel, 08–16 mm | 687.5 | 685.7 |
| Aggregate content | 69.0% | 68.8% |
| Apparent sand content | 43.4% | 43.4% |
| Paste content | 25.5% | 25.1% |
| Mortar content | 55.4% | 54.9% |
| Water–cementitious materials ratio | 0.307 | 0.480 |

were cast in special wooden water-tight molds manufactured for this purpose. The groove and the notch in the WST-specimens were cast using tapered PVC inserts. The concrete was compacted on a table vibrator for 2 min at 50 Hz.

The dimensions of the cylinders were $\varnothing 100 \times 200$ mm. The loading strips were made of wooden fibreboards and they were 10 mm wide and 5 mm thick. The geometry of the WST-specimens are shown in Fig. 2a. The side length of the fundamental WST-cube is $L = 100$ mm, and the thickness $t = 100$ mm. The height of the ligament is $h = 50$ mm, while the splitting load is applied at $(d_1, d_2) = (40, 85)$ mm. The length of the notch is $a_0 = 28$ mm. Fig. 2 shows the mean width of the notch, $a_m = 4.5$ mm, while the real notch was a little tapered in order to ensure easy demolding.

The specimens were covered with plastic sheets immediately after casting and stored in the lab until testing. Only 15 min elapsed from addition of water and until the final covering of the specimens. Specimens that were used for tests before 24 h were taken directly from the molds. At 24 h, the specimens were demolded and stored at 100% RH and laboratory temperature (20 °C) until testing. The specimen temperature at the time of each test was recorded using a thermocouple cast into the center of dummy specimen with dimensions corresponding to the cylindrical specimens.

Handling and testing of very early-age concrete using the WST-configuration is easy compared to testing with beams. This is in fact one of the major advantages with the WST-setup. For specimens tested at ages later than 10 h, the influence of self-weight was small compared to the strength of the specimen. Self-weight only played a role at 8 and 10 h. However, in order to include the effect properly, self-weight was considered in the modelling for all samples.

Fig. 5 shows the experimental setup, which except for minor corrections corresponds to the setup described in [11], see also the principal drawing in Fig. 1. Fig. 5 shows how the dead weight on the specimen has been minimized by mounting the wedge to the upper loading plate. It is also illustrated how unwanted restraints are prevented by a rotational joint (roller bearings) above the wedge combined with a rotational joint (a rectangular brass bar) below the specimen perpendicular to the first joint. Finally, a ball joint has been used below the brass bar to make sure that the specimen with loading plates will fit into the wedge. A clip gage measuring the midpoint CMOD at load line is also seen in Fig. 5.

The wedge split tests were conducted using a constant displacement rate of the wedge of 0.01 mm/s. In this way, the peak load was reached within 2 min for all experiments. The rate was increased to 0.04 mm/s at the end of the experiments. The split tests were conducted such that the peak load was reached within approximately 1 min. The experimental programme conducted in this paper comprised in total 40 wedge splitting tests and 40 split cylinders.

Fig. 5. Experimental setup.

## 4. Results and discussion

Fig. 6 shows the fracture surfaces for samples at very early age (10 h) and for mature samples. At 8–10 h, the paste was so weak that fracturing of the specimen by hand would not be a problem. The fracture surface was very rough at this age, and absolutely no aggregates were fractured. At 28 days the picture had completely changed. The crack had run directly through the aggregates and the fracture surface was much more smooth.

The load–CMOD curves for the same specimens are shown in Fig. 7. These graphs demonstrate the performance of the model and of the inverse analysis. Furthermore, it is seen that the tails of the curves are very different, indicating high brittleness for the matured sample. But also the early-age sample shows pronounced brittleness in the first part of the curve, since this part of the curve is very steep.

Fig. 8a shows the development in the tensile strength, $f_t$. The observed development in tensile strength follows the body of knowledge and the small scatter in the tensile strength is very promising for the method. The second strength gain from 100 h and afterwards is probably a result of activation of the class F fly ash. The development of modulus of elasticity seen in Fig. 8b shows some scatter and furthermore, a drop in $E$ is seen

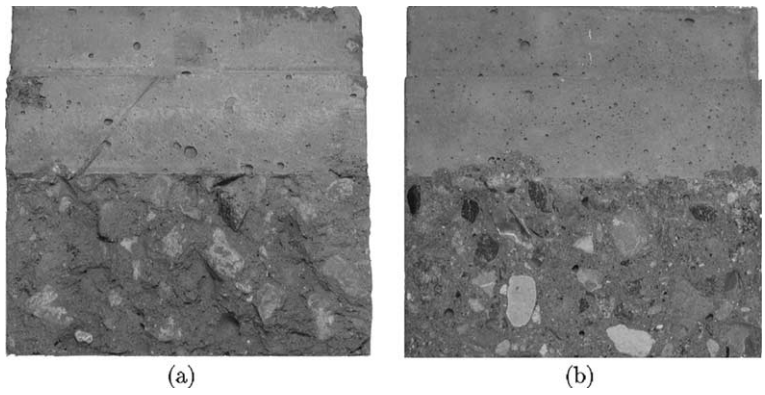


Fig. 6. Fracture surface for $w/c = 0.307$ at 10 h (a) and at 28 days (b). Aggregates started fracturing at 28 h.

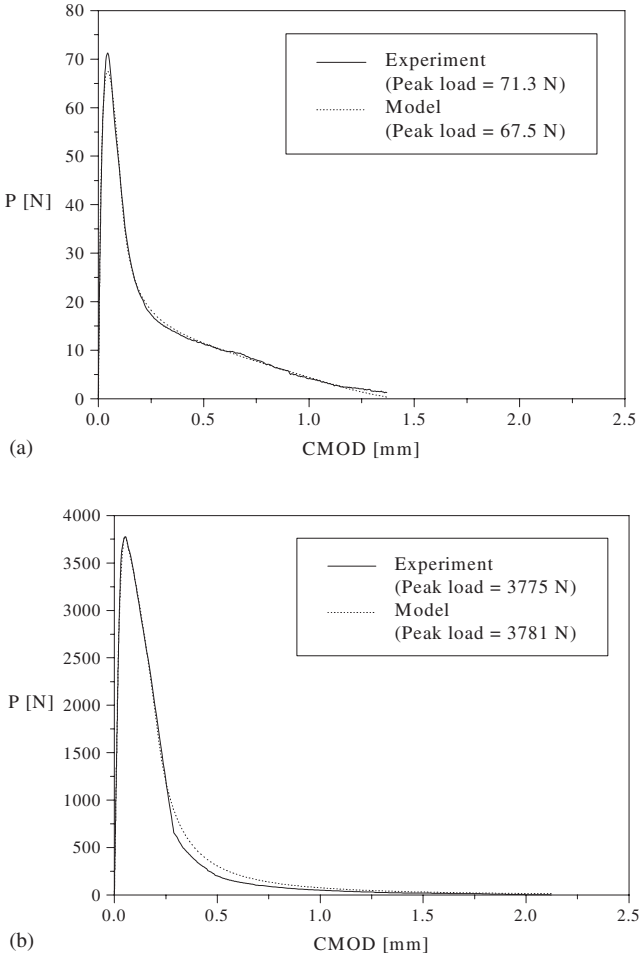


Fig. 7. Load–crack mouth opening displacement curves for $w/c = 0.307$ at 10 h and at 28 days.

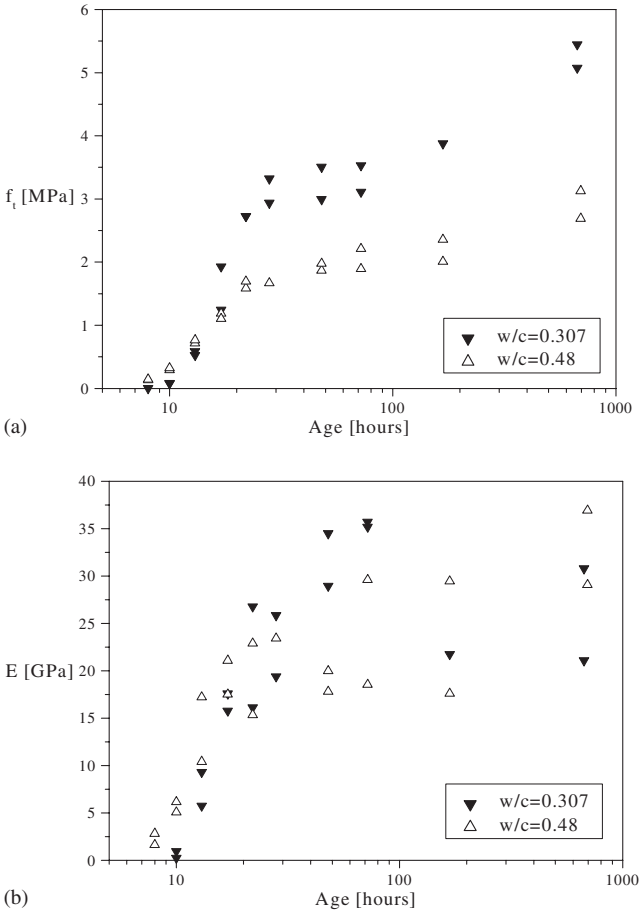


Fig. 8. Development in tensile strength (a) and modulus of elasticity (b).

for the low water to cementitious materials ratio concrete. However, except for these observations, the development roughly follows the tensile strength gain, which is expected. The large scatter probably arises from the fact that this test method is not the optimal choice for the determination of the modulus of elasticity. In this test, material near the notch will play a large role on the small elastic deformations, and small changes due to e.g. aggregates or surface cracks may affect the determination significantly. Self-desiccation micro-cracks at 28 days might for example have changed the stiffness of the material near the notch, resulting in a lower value for $E$. In general, the results on the determination of $f_t$ and $E$ follow the literature, see e.g. [5]. Their results also seems to indicate a drop in the modulus of elasticity at

28 days. It is also noted that some of the scatter found in the present work probably is due to the ligament size versus the maximum aggregate size since the ligament is $100 \times 50$ mm while the maximum aggregate size is 16 mm.

Interesting behavior is seen in the development of the slopes of the stress–crack opening relationship (Fig. 9). The first slope, $a_1$ reaches high values in early age whereafter it decreases to values expected for mature concrete. This behavior is surprising since it indicates a more brittle behavior for early-age concrete than for mature concrete in the first part of the stress–crack opening relationship. This steep drop in the first part of the curve is probably associated with the poor cross-linking and interconnection of the hydration products in very early age. This results in a poor ability to withstand a propagating crack driven by the release of elastic energy stored in the specimen on the loading branch. The development of $a_1$ is in agreement with the literature, see [5], where $a_1$, however determined at later ages (2–28 days), also has been found to decrease. The second slope of the stress–crack opening relationship, $a_2$, is seen to be almost constant in early age, whereas it increases for the low water to cementitious materials ratio concrete as this mix matures. The latter mechanism is probably due to the high strength of the matured paste in this concrete. The paste is simply stronger than the aggregates, and thus, no aggregate bridging exists. In fact, the stress–crack opening relationship in these cases can probably be described with a mono-linear curve. This statement is confirmed from the results for $b_2$ where high values are found for matured low water to cementitious materials ratio concrete, see Fig. 10a.

The development in $b_2$, see Fig. 10a is not clear due to some scatter. However, for the low water to cementitious materials ratio concrete the trend is an increase with age. The governing mechanism is most likely a decrease in the ductility of aggregate pull-out. As the paste matures, the pull-out failure will be more and more brittle, and finally the aggregates will start to rupture, resulting in the mono-linear curve as described above. Fig. 10b shows the development in fracture energy with age. The development of this property is in agreement with the majority of work in the literature, see e.g. [2,4,5]. Like in these papers it is found that the fracture energy increases with age. Fig. 10b also shows how the fracture energy is higher for the low water to cementitious materials ratio concrete than for the high

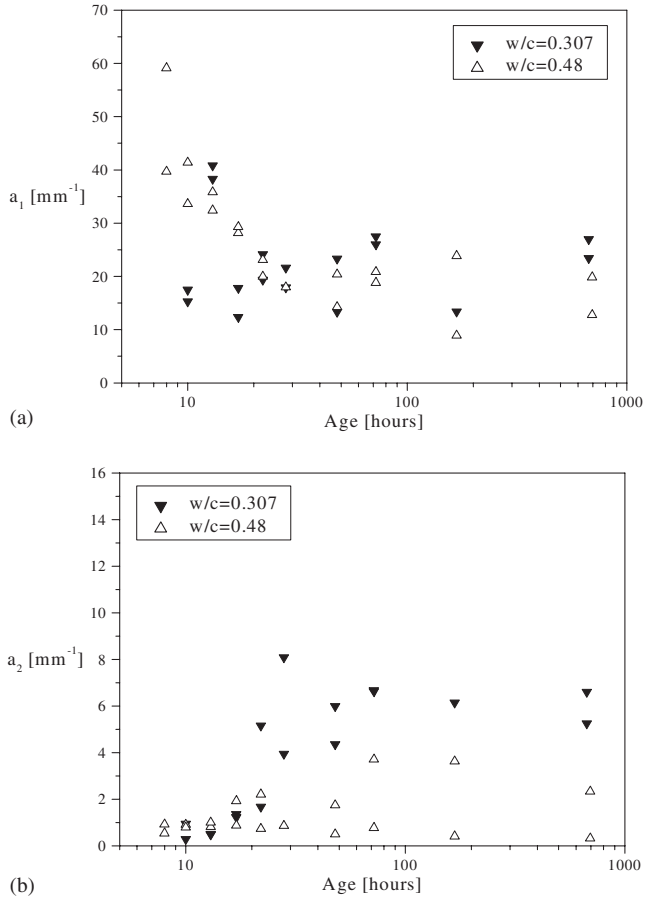


Fig. 9. Development in slopes of the bilinear stress–crack opening relationship.

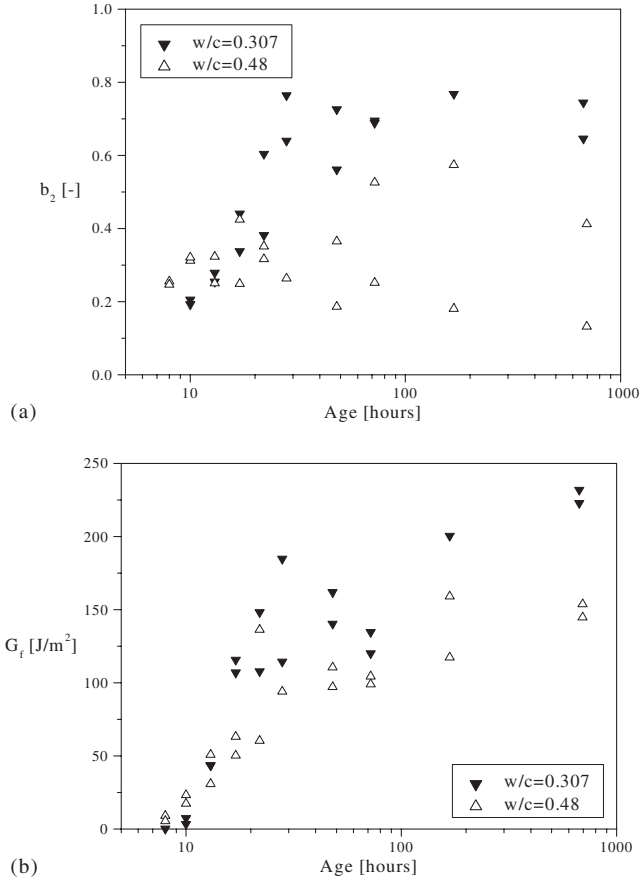


Fig. 10. Development in $b_2$ (a) and fracture energy (b).

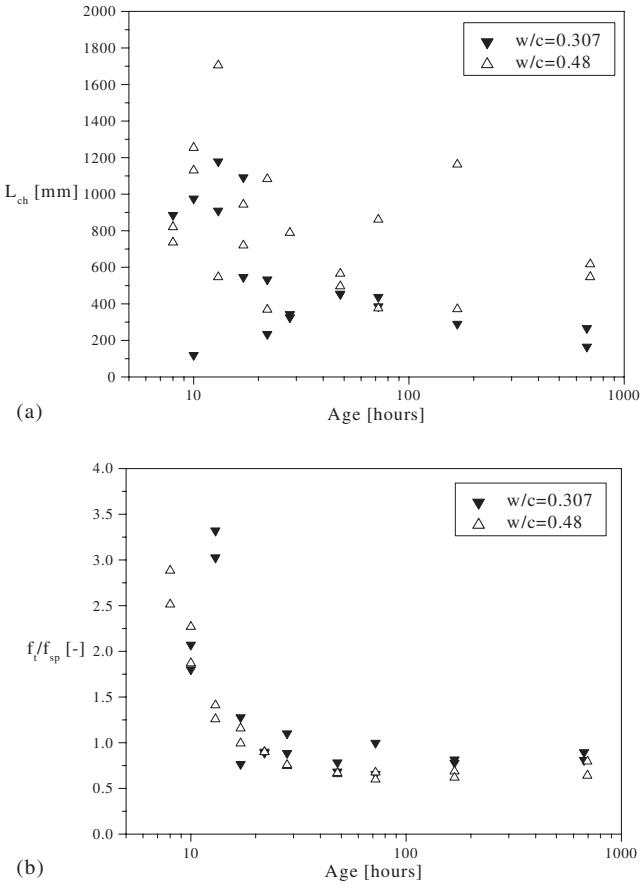


Fig. 11. Development in characteristic length and $f_t/f_{sp}$-ratio.

water to cementitious materials ratio concrete, which is in agreement with [2,5] where similar investigations were performed.

Fig. 11a shows the development in characteristic length. The characteristic length is calculated using Hillerborgs equation [1]:

$$l_{ch} = \frac{EG_f}{f_t^2} \tag{9}$$

The general trend in the development of the characteristic length despite the scatter, is showing a decrease. However, intermediate periods of low values are found on the graph. This indicates that early-age concrete might at certain ages be more brittle than mature concrete, a result that was also found in the literature, e.g. [3,8].

The development of the ratio between the tensile strength and the splitting tensile strength, $f_{sp}$, is shown in Fig. 11, where $f_{sp}$ is calculated on basis of the standard linear elastic formula:

$$f_{sp} = \frac{2P_{max}}{\pi BD} \tag{10}$$

Most strikingly, it is clearly seen from Fig. 11b, that the splitting tensile strength is not a good measure of the tensile strength in early age. Here, the ratio reaches higher values than expected at a first glance. This is due to the failure mechanism of the splitting cylinder specimen. While mature samples in this test program were failing under formation of a single tensile crack at the center plane, samples at early age developed large compressive failure cones. In fact, for some samples at very early age, the cones were intersecting at the center of the specimen. This shows clearly that the split cylinder is failing in *compression* rather than in *tension* for samples at such early ages. Thus, the specimen is not well suited for determining tensile strength at early age, which confirms the results by Østergaard et al. [20]. For mature concrete however, as the figure shows, a constant ratio between the true and the split tensile strength develops at a value of approximately $f_t/f_{sp} \approx 0.7$–$0.8$ which is expected from the body of knowledge. Thus, other methods must be applied for the determination of the tensile strength in early age, for example the method described in this paper, or e.g. the uniaxial tension test. This conclusion is supported by the findings of Altoubat [21] who found that the ratio between the uniaxial tensile strength and the split tensile strength is changing within the first 100 h after casting.

Fig. 12a and b show some examples of stress–crack opening relationships at different ages. These graphs help giving an overview over the development of properties. The normalized graphs show how $a_1$ is decreasing with age and how the aggregate bridging action has almost vanished at 28 days. The graphs in Fig. 12b show how the fracture energy, given by the area under the curves, is increasing with age.

## 5. Conclusion

A basis for the determination of the fracture mechanical properties, including the stress–crack opening relationship for early age, and for mature, concrete has been established. The conclusions are based on analytical models describing the fracture mechanical behavior of concrete, and on finite element models which have confirmed the analytical results. This model and the inverse analysis method developed has shown its applicability to concrete and good results have been obtained.

For early-age concrete, it was indicated that the splitting tensile test is not a well suited test for determination of tensile strength for concrete younger than 24 h. In this period other methods should be applied.

From the wedge splitting tests it was shown that the fracture energy of concrete increases with age. This increase was accompanied with an increase of tensile strength and modulus of elasticity. However, the ductility of the concrete in terms of the characteristic length

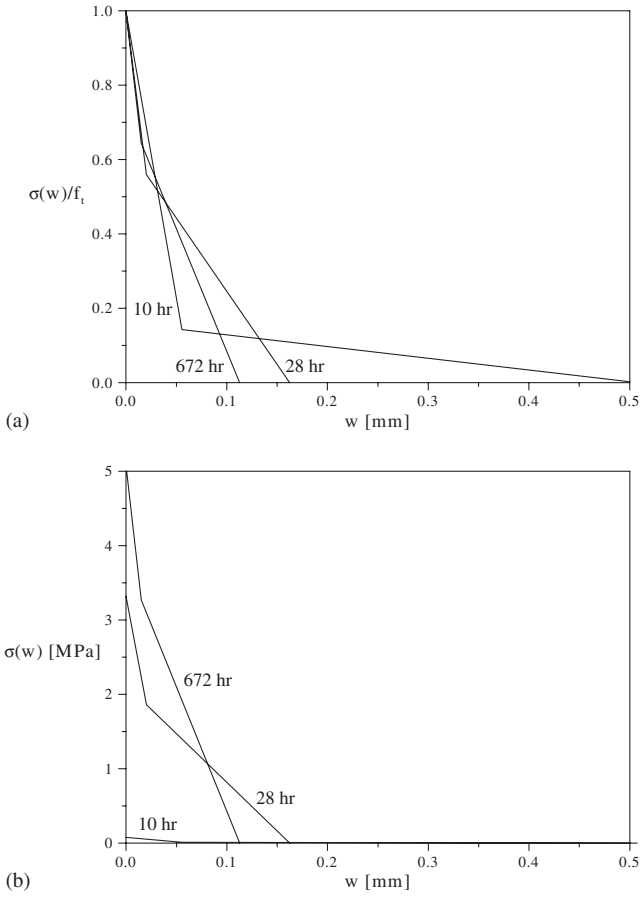


Fig. 12. Examples of stress–crack opening relationships for different ages; normalized curves (a) and absolute curves (b) for $w/c = 0.307$.

was found to decrease. Overall, the results confirm the basic trends observed in literature.

## Appendix A

This appendix contains the derivation of Eqs. (6) and (7). The derivations may also be found in [13,16]. The mean strain, $\varepsilon^*$ of an incremental strip in the hinge element is readily obtained since the boundary planes of the hinge element are assumed to be straight:

$$\varepsilon^* = 2(y - y_0)\frac{\varphi}{s} \tag{A.1}$$

where $y_0$ is the position of the neutral axis. It is also simple to express the elongation of the incremental strip as the sum of the elastic deformation and the crack opening:

$$u(y) = s\varepsilon^* = s\frac{\sigma_w(w(y))}{E} + w(y) \tag{A.2}$$

Here, the crack opening in the incremental strip, $w(y)$, and the corresponding crack stress, $\sigma_w(w(y))$, have been introduced. By combining (A.1) and (A.2) we may write:

$$\sigma_w(w(y)) = (2(y - y_0)\varphi - w(y))\frac{E}{s} \tag{A.3}$$

$\sigma_w(w(y))$ is assumed bilinear and thus also given by

$$\sigma_w(w(y)) = f_t(b_i - a_i w(y)) \tag{A.4}$$

Eqs. (A.3) and (A.4) may be solved for $\sigma_w(w(y))$ and $w(y)$:

$$w(y) = \frac{2(y - y_0)\varphi - \zeta_i}{1 - \beta_i} \tag{A.5}$$

$$\sigma_w(w(y)) = \frac{\zeta_i - 2(y - y_0)\varphi\beta_i}{1 - \beta_i}\frac{E}{s} \tag{A.6}$$

where $\beta_i = (f_t a_i s)/E$ and $\zeta_i = (f_t b_i s)/E$. $\delta_{COD}$ is now determined by selecting $y = h$, and it is simple to show that

$$\delta_{COD} = w(h) = \frac{sf_t}{E}\frac{1 - b_i + 2\alpha\theta}{1 - \beta_i} \tag{A.7}$$

The opening due to the distance between the load line and the bottom of the notch, $\delta_g$, see also Eq. (7), may be calculated from Eq. (A.5). It is assumed that $\delta_g$ is governed by the mean angle of the crack surfaces relative to the vertical line of symmetry. This angle, denoted the crack angle, $\varphi_{cr}$, is for all phases given by

$$\varphi_{cr} = \frac{\delta_{COD}}{2\alpha h} \tag{A.8}$$

However, due to an artifact of the model, the angle of the crack faces are not equal to zero at crack initiation, instead they instantly assume a certain angle, $\varphi_{cr}^0$. This angle may be derived by differentiating Eq. (A.5):

$$\varphi_{cr} = \frac{1}{2}\frac{\partial w(y)}{\partial y} = \frac{\varphi}{1 - \beta_i} \tag{A.9}$$

Thus, $\varphi_{cr}^0$ is given by

$$\varphi_{cr}^0 = \frac{\varphi_{0-I}}{1 - \beta_1} \tag{A.10}$$

where $\varphi_{0-I}$ represents the rotation of the hinge at initiation of the crack. The corrected crack angle is given by $\overline{\varphi}_{cr} = \varphi_{cr} - \varphi_{cr}^0$ and thus, $\delta_g$ is given by

$$\begin{aligned}\delta_g &= 2\overline{\varphi}_{cr}(b - h)\\ &= 2(b - h)\left(\frac{\delta_{COD}}{2\alpha h} - \frac{sf_t}{hE}\frac{\theta_{0-I}}{1 - \beta_1}\right)\end{aligned} \tag{A.11}$$

where $\varphi$ in the latter expression has been replaced by the normalized angle $\theta$.

## References

[1] Hillerborg A, Modéer M, Petersson PE. Analysis of crack formation and crack growth in concrete by means of fracture mechanics and finite elements. Cem Concr Res 1976;6:773–82.
[2] Petersson PE. Fracture energy of concrete: practical performance and experimental results. Cem Concr Res 1980;10:91–101.

[3] Brameshuber W, Hilsdorf HK. Development of strength and deformability of very young concrete. In: Fracture of concrete and rock. Springer-Verlag; 1987. p. 409–21.
[4] Brameshuber W. Bruchmechanische Eigenschaften vaon jungem Beton. PhD thesis, Schriftenreihe des Instituts für Massivbau und Baustofftechnologie, J. Eibl & H.K. Hilsdorf, 1988.
[5] Wittmann FH, Roelfstra PE, Mihashi H, Huang Y-Y, Zhang X-H. Influence of age of loading, water–cement ratio and rate of loading on fracture energy of concrete. Mater Struct 1987;20:103–10.
[6] Zollinger DG, Tang T, Yoo RH. Fracture toughness of concrete at early ages. ACI Mater J 1993;90(5):463–71.
[7] Schutter GD, Taerwe L. Fracture energy of concrete at early ages. Mater Struct 1997;30:67–71.
[8] Gettu R, Garcia-Álvarez VO, Aguado A. Effect of aging on the fracture characteristics and brittleness of a high-strength concrete. Cem Concr Res 1998;28(3):349–55.
[9] Hariri, K. Bruchmechanisches Verhalten jungen Betons. Laser-Speckle-Interferometrie und Modellierung der Rißprozeßzone. Number 509. Deutscher Auss-chuß für Stahlbeton, 2000.
[10] Linsbauer HN, Tschegg EK. Fracture energy determination of concrete with cube shaped specimens. Zement Beton 1986;31:38–40 (in German).
[11] Rossi P, Brühwiler E, Chhuy S, Jenq Y-S, Shah SP. Fracture properties of concrete as determined by means of wedge splitting tests and tapered double cantilever beam tests. In: Shah SP, Carpinteri A, editors. Fracture mechanics test methods for concrete. Chapmann & Hall; 1991. p. 87–128 (Chapter 2).
[12] Ulfkjær J, Krenk S, Brincker R. Analytical model for fictitious crack propagation in concrete beams. J Eng Mech 1995;121(1):7–15.
[13] Olesen JF. Fictitious crack propagation in fiber-reinforced concrete beams. J Eng Mech 2001;127(3):272–80.
[14] Stang H, Olesen JF. A fracture mechanics-based design approach to frc. In: Proceedings of the 5th RILEM Symposium on Fiber-Reinforced Concretes (FRCs), BEFIB 2000.
[15] Stang H, Olesen JF. On the interpretation of bending tests on frc materials. In: Proceedings of FRAMCOS-3, Fracture Mechanics of Concrete Structures, Freiburg, Germany, vol. I. Aedificatio Publishers; 1998. p. 511–20.
[16] Østergaard L, Olesen JF, Stang H, Lange DA. Interpretation and inverse analysis of the wedge splitting test. J Eng Mech, submitted for publication.
[17] Tada H, Paris P, Irwin G. The stress analysis of cracks handbook. Missouri, USA: Paris Productions Incorporated; 1985.
[18] Hauggaard AB, Damkilde L, Hansen PF, Hansen JH, Christensen SL, Nielsen A. HETEK, control of early age cracking in concrete, phase 3: creep in concrete. The Danish Road Directorate; 1997.
[19] Hauggaard AB, Damkilde L, Hansen PF, Hansen JH, Christensen SL, Nielsen A. HETEK, control of early age cracking in concrete, phase 4 and 5: material modelling, continuum approach. Danish Road Directorate; 1997.
[20] Østergaard L, Olesen JF, Stang H. Modelling simultaneous tensile and compressive failure modes of the split cylinder test. In: Proceedings of the 14th Nordic Seminar on Computational Mechanics. Lund, Sweden: KFS; 2001. p. 193–6.
[21] Altoubat SA. Early age stresses and creep-shrinkage interaction of restrained concrete. PhD thesis, University of Illinois at Urbana-Champaign, Civil and Environmental Engineering, Urbana, IL, USA, 2000.